Engineering Structures 150 (2017) 153–165

Contents lists available at ScienceDirect

Engineering Structures

journal homepage: www.elsevier.com/locate/engstruct

Infill walls with confining elements and horizontal reinforcement: An experimental study

J.M. Leal G. [a], J.J. Pérez Gavilán [b,*], J.H. Castorena G. [c], J.I. Velázquez D. [d]

[a] Instituto de Ingeniería de la UNAM, Av. Universidad 3000, CU, CP 04510 México D.F., Mexico
[b] Ingeniería Estructural, Instituto de Ingeniería de la UNAM, Av. Universidad 3000, CU, CP 04510 México D.F., Mexico
[c] Faculty of Engineering Los Mochis, Universidad Autónoma de Sinaloa, Fuente de Poseidón y Ángel Flores, Jiquilpan, CU, CP 81223 Los Mochis, Sinaloa, Mexico
[d] Faculty of Engineering Culiacán, Universidad Autónoma de Sinaloa, Calz. Las Americas Nte, CU, 80013 Cuiacán de Rosales, Sinaloa, Mexico

ARTICLE INFO

Article history:
Received 8 March 2017
Revised 27 May 2017
Accepted 14 July 2017
Available online 24 July 2017

ABSTRACT

An experimental investigation of the global behavior of reinforced-concrete frames infilled with masonry walls was conducted. The study variables were the wall/frame stiffness ratio, the use of confining elements and the use of horizontal reinforcement. Six specimens scaled 1:2 were tested. The results indicate that the wall/frame stiffness ratio has an important effect on the cracking strength of the walls and the maximum shear strength of the system. Moreover, the contribution of horizontal reinforcement to lateral strength depends on the wall/frame stiffness ratio. Confining elements surrounding the infill walls do not increase the lateral strength or displacement capacity of the system; however, they enhance the out-of-plane stability of the wall and the contact conditions between the wall and frame.

1. Introduction

Reinforced concrete frames infilled with masonry walls are designed considering the frame as the main resistant element. The contribution of the wall is usually regarded as a resistance reserve. However, this consideration does not always lead to safer designs [4]. Past seismic experiences have indicated that, depending on the infill walls' physical and mechanical characteristics, its components and reinforcement conditions may lead to beneficial or adverse effects on the behavior of the structure. Hamburger and Meyer [8] and Murty and Jain [14] noted beneficial effects of frames infilled with masonry walls during the 1906 San Francisco earthquake and moderate earthquakes in India. On the other hand, Saatcioglu et al. [19] noted the poor performance of reinforced-concrete-infilled frames, the primary structural system used in Turkey, during the Kocaeli 1999 earthquake [18].

At the global level, infill walls significantly increase the lateral stiffness and strength of the structure and improve the system's capacity for energy dissipation. At the local level, along the contact length, between wall and frame, shear and compressive stresses are generated. The contact length of the interface depends on the relative stiffnesses of the masonry wall and the frame. The presence of infill walls transforms the internal force diagrams obtained from an analysis of the structure without walls. Normal stresses are highly concentrated at the corners. This concentration causes a significant increase in the bending moment and the shear force acting on the frame [3].

Analytical models based on the concept of the equivalent diagonal strut that consider the structure as an equivalent braced-frame system with a diagonal compression strut replacing the infill wall, provide an accurate prediction of the global behavior of the system [10]. In these analytical models, numerous empirical equations are employed, through which researchers have tried to relate the mechanical and geometrical properties of infilled frames with some structural parameters, such as lateral stiffness, lateral strength and the contact length between the frame and the infill wall. The above mentioned equations are functions of dimensionless parameters, such as the one proposed by Stafford-Smith and Carter [20] and the one proposed by Bazán [1], that express the wall/frame stiffness ratio.

The behavior of infilled frames subjected to lateral loads has been related to the ratio of the story shear strength provided by the infill walls to the story shear strength provided by the bare frames. If the infill walls are too robust, they could induce soft-story behavior of the frame. Ravichandra and Klinger [18] concluded, based on a numerical investigation for steel infilled frames, that "If the infill strength ratio (the ratio of story shear strength of infills to the story shear strength of bare frame) is less than approximately 0.35, the presence of infills does not change the failure mechanism, which involves hinging in beams and at column bases". However, "When the infill strength ratio reaches

* Corresponding author.
E-mail addresses: martin_leal2@hotmail.com (J.M. Leal G.), jperezgavilane@iingen.unam.mx (J.J. Pérez Gavilán), humbertocastorena@yahoo.com.mx (J.H. Castorena G.), juanv@uas.edu.mx (J.I. Velázquez D.).

http://dx.doi.org/10.1016/j.engstruct.2017.07.042
0141-0296/

approximately 0.35, the presence of the infill begins to change the failure mechanism of the frame, from hinging in beams and at column bases, to story mechanisms involving column hinging at multiple levels of the lower stories".

In most cases, infill walls consist of unreinforced masonry walls. The main reason for not using confining elements is that it is considered that the frame's elements already provide confinement and consequently there is no need for additional elements for that purpose. However, the frame separates from the wall for small lateral displacements, meaning that the confining effect is lost early in the response of the system to an earthquake. On the other hand, if the lateral stiffness of the confining elements is small relative to that of the masonry panel, the confining elements do no separate from the wall, maintaining its confining effect all the way to the system failure [17]. Other reasons for not using confining elements are their added cost and the difficulty of constructing the upper tie beam that should be in contact with the frame's beam.

Unreinforced masonry walls have very limited drift capacity, and their strength degrades rapidly after the first diagonal cracks due to tension appear. Confined masonry is an alternative that considerably increases the displacement capacity of the walls. Meli [13] described the experimental behavior of masonry walls subjected to lateral alternating loads, including walls with tie columns and bond beams and interiorly reinforced walls (reinforced masonry partially grouted using units with thickness typically less than or equal to 150 mm). Based on experimental results and on the direct observation of the effect of earthquakes, he concluded that walls strengthened with tie columns and tie beams have better behavior than unreinforced or interiorly reinforced walls, judging by the large ductilities that the walls may reach in spite of important damage in the walls and in the tie columns. In addition, tie columns also provide a considerable increase in the out-of-plane stability of the walls.

Because the frame is constructed before the infill walls, it is difficult to provide horizontal reinforcement in the wall, as such reinforcement should be anchored in the columns and cannot be lapped [7]. However, horizontal reinforcement is potentially useful, as in confined masonry walls, it dramatically increases their displacement capacity and significantly increases their strength. If tie columns are included as part of the infill wall, they are cast, and the concrete is poured after the walls are built. Intermediate tie columns should be included for confined masonry walls so that their spacing is less than 1.5 H and 4 m [7]. Because of the construction sequence, tie columns allow the inclusion of horizontal reinforcement that can be properly anchored without lapping.

To estimate the forces in the infill wall, the Canadian standard [2] uses the equivalent diagonal method for the analysis, which is based on the model proposed by Stafford-Smith and Carter [20]. In this model, the cross section's effective width of the diagonal element is determined based on the wall-to-frame stiffness ratio but cannot be larger the diagonal length divided by 4, a limit value that often governs the effective width. The Canadian standard considers several failure modes for the infill wall: crushing of the diagonal strut, buckling based on the slenderness of the diagonal and the shear failure that can occur through sliding along intermediate joints or diagonal tension. The sliding strength is based on a Coulomb frictional model that is dependent on the vertical stress acting in the sliding plane, which is computed with the vertical component of the force in the diagonal, and a friction coefficient. The shear strength due to diagonal tension is provided by the strength of the masonry to tension, expressed as the square root of the compressive strength ($\sqrt{f'_m}$), and the horizontal reinforcement, which is assumed to be properly anchored in fully grouted internal cells of the wall.

The New Zealand standard [15] specifies that "masonry in-filled frames shall be designed as elastically responding structures, unless a special study is carried out to determine the available structural ductility, μ.". Although a friction failure is considered, the code includes in its comments that, "virtually all considerations of shear are intended to prevent diagonal tension failures".

The Mexico City code [7] only considers failure due to diagonal tension with an expression that is specific to infill walls. The given expression ignores the added strength due to the vertical load in the wall, which is considered to be transferred by the frame's columns.

In the present study, an experimental program was conducted to investigate the behavior of concrete frames infilled with masonry walls using confining elements and horizontal reinforcement. Unlike the many studies that used square infill walls, a small height-to-length aspect ratio was used, which was considered to be more representative of the infill walls used in practice. The main results show that the frame size has a significant effect on the lateral strength of the system; the effect of horizontal reinforcement on the strength of the system depends on the frame/wall stiffness ratio. The inclusion of confining elements has little impact on the lateral strength and displacement capacity of the infilled frames. Details of the testing procedure and the results are given next.

2. Experimental program

2.1. Prototype buildings

Two prototype buildings were analyzed and designed according to the Mexico City code for the design of concrete structures [6]. The structures had the same plan configuration (Fig. 1); however, to obtain different column sizes, they had three and six stories. The buildings had three bays of 7 m in each direction and the inter-story height was kept constant at 3 m. Frames A and D, parallel to the Z direction, were infilled with masonry walls. In the X direction, concrete walls were located in the frames of axes 1 and 4, between axes B and C.

The analyses of the buildings were conducted with static lateral forces varying linearly with height, using a seismic coefficient

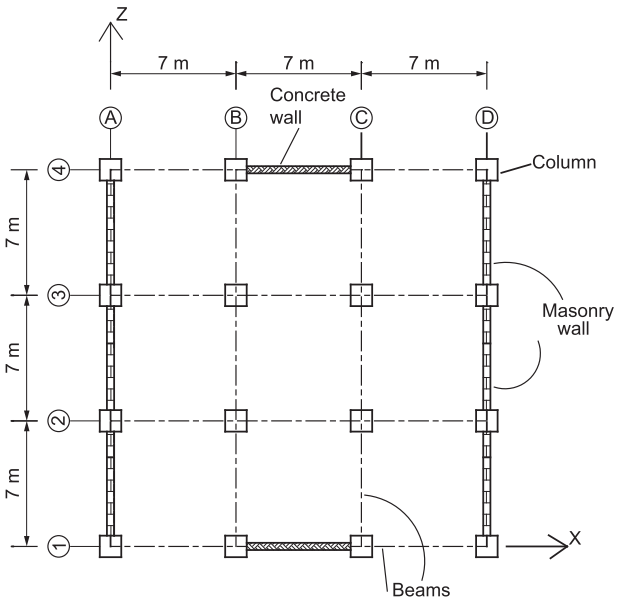

Fig. 1. Floor plan of the prototype building.

equal to 0.40 and designed using a seismic reduction factor R = 3 (in the Mexico City code, Q = 3). The frames were designed so that they were capable of resisting 80% of the total seismic forces, without the contribution of the infill walls.

2.2. Specimens

The specimens were built based on the central infilled bay of the lower story of the prototype buildings. Due to space limitations in the laboratory, the specimens were scaled 1:2. The main criterion for the scaling was to keep the shear and axial stresses in the model equal to those of the prototype so that the mechanical properties of the materials could be preserved in the models. The percentage of longitudinal reinforcements was also preserved in the model. Material properties are shown in Table 1.

Six specimens were built in pairs. Both specimens in each pair had identical characteristics, except for the size of the frame members, since in one case they represented the frame elements of the three-floor prototype building while in the other they corresponded to that of the building with six stories.

After each specimen in the pair was tested, they were destroyed and a new pair of specimens was built in the same place. In the first pair of specimens, specimens MD3NSR and MD6NSR, no confining elements and no horizontal reinforcement were provided. In the second pair (specimens MD3N and MD6N), tie columns and tie beams were added to the infill walls. The dimensions of these concrete elements were 65 × 100 mm. Finally, for the third pair (specimens MD3NRH and MD6NRH), horizontal reinforcement consisting of a 4 mm-diameter bar every six courses, anchored in the tie columns, was added to the infill walls.

Figs. 2 and 3 illustrate the details of the reinforcement and dimensions of the specimen frames corresponding to the prototype buildings with three and six stories, respectively. The longitudinal reinforcement in columns and beams consisted of 12.7 and 9.5 mm-diameter bars with 6 mm-diameter stirrups, all of which were commercially available. In the columns, the reinforcement percent ratios were 3.3% and 2.4%. The spacing of the stirrups was reduced at each end of the frame elements so that plastic hinges could develop.

Infill walls were made of brick units with nominal dimensions of 25 × 65 × 125 mm, which were specially manufactured for the experimental campaign using the same procedure and clay used for the full-size units that are typical in the region. Mortar joints were 7 mm thick. The global dimensions of the wall corresponding to the three-story building were 1375 mm in height and 3325 mm long, having an aspect ratio equal to 0.414. The overall dimensions of the wall corresponding to the six-story building were 1350 mm in height and 3250 mm long, having an aspect ratio H/L equal to 0.415. Details of the horizontal reinforcement and dimensions of the infill walls are shown in Fig. 4.

2.3. Construction of the specimens

The specimens were built in pairs. Two reusable reinforced-concrete foundations were built, each of which had vertical openings near the end in order to anchor the columns of the frames (Fig. 5a). The foundation reinforcement crossed the openings and the reinforcement of the columns was tied to it. After the specimen was tested, concrete in the openings and reinforcement of the columns was removed and the foundation was reused for the next specimen.

For each specimen, the frame was built first and, after seven days of concrete setting, was infilled with the masonry wall. Monolithically with the beam, a 100 mm-thick slab was built to connect the specimen to the system used to apply the lateral load. For walls with confining elements, the bottom tie beam was built over the foundation, into which the tie columns were anchored (Fig. 5b). Tie columns were cast after the masonry wall was built. To ensure that frame and wall were in contact, the upper tie beam was built using the casting system shown in Fig. 5c. Concrete with slump greater than 180 mm was poured through windows, which provided enough hydrostatic pressure to fill the tie beam completely. When the concrete was set, the excess was removed with a mechanical device. At the top of each column, a 19.1 mm-thick plate was anchored to hold the system used to apply the vertical load. In specimens without confining elements, the wall was placed directly on the foundation and masonry was in contact with the frame, with the same mortar used for bed joints.

2.4. Material properties

During construction of the specimens, material samples were obtained from the same concrete and mortar mixtures used to build the different elements. The specimens were built in pairs so that material samples would correspond to both specimens in the pair. Table 1 shows average values of the results of material tests for each pair of specimens.

Concrete strength and elastic modulus, f'_{cf} and E_{cf} for the frame's concrete and f'_{cc} and E_{cc} for confining element's concrete, were obtained through standard cylinder tests. For each pair of specimens, twelve concrete samples were obtained, eight samples from the frame and four samples from the confining elements. Each concrete sample consisted of three cylinders.

The masonry's properties, including compressive strength, f_m, diagonal compressive strength, v_m, and elastic modulus, E_m, were investigated through the corresponding standard Mexican tests [16], similar to ASTM C1314 and ASTM E519 tests. Six samples for each masonry property were tested for each pair of specimens.

Mortar compressive strength, f_j, was obtained through 50 × 50 mm cubes tests. For each pair of specimens, eighteen mortar samples were obtained. Each mortar sample consisted of three

Table 1
Material properties.

Specimen	Frames		Confining elements[+]		Masonry			Mortar[++]	Units
	f'_{cf} (MPa)	E_{cf} (MPa)	f'_{cc} (MPa)	E_{cc} (MPa)	f_m (MPa)	v_m (MPa)	E_m (MPa)	f_j (MPa)	f_p (MPa)
MD3NSR MD6NSR	26.12	22402	–	–	3.49	0.63	725	16.82	9.36
MD3N MD6N	19.03	19490	15.07	17220	3.40	0.53	703	15.01	9.36
MD3NRH MD6NRH	19.95	19719	13.30	15661	3.34	0.59	693	8.01	9.36

[+] Maximum gravel size was 12.7 mm.
[++] Sand modulus of fineness was 2.6.

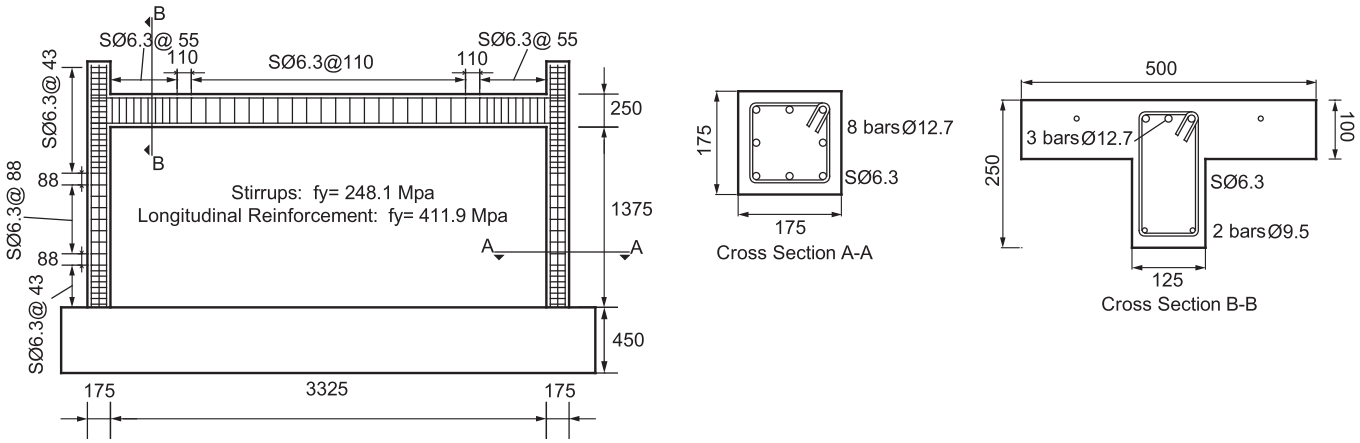

Fig. 2. Details of reinforcement and dimensions (in millimeters) of the frame corresponding to the prototype building with three stories.

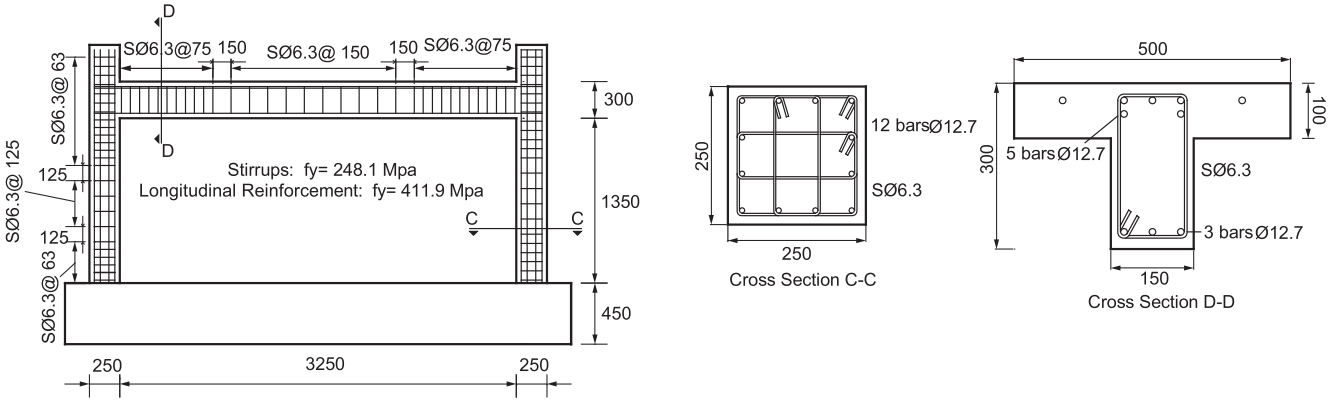

Fig. 3. Details of reinforcement and dimensions (in millimeters) of the frame corresponding to the prototype building with six stories.

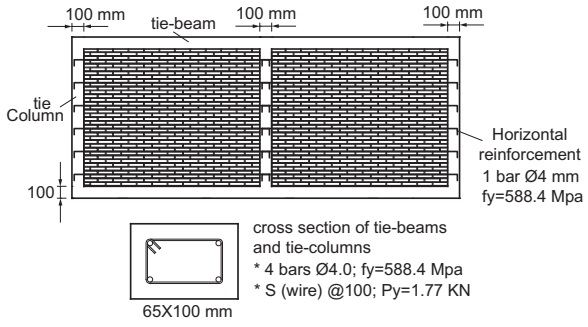

Fig. 4. Details of reinforcement and dimensions (in millimeters) of the infill wall with confining elements.

cubes. The average compressive strength of the masonry units, f_p, was obtained with ten tests of individual units.

2.5. Test setup and instrumentation

The setup used to apply the vertical and lateral loads during the tests is shown in Fig. 6. The vertical load was applied directly to the frame columns. It represented the gravity loads of the upper stories and the dead load of the lower floor. The load was applied with hydraulic actuators, which reacted against a steel beam anchored to the foundation with tensors on each side of the wall (Fig. 6b). The weight of the steel beam on top of the frame beam, used to transfer the lateral load, represented the live load of the lower story. The lateral load was applied using two hydraulic actuators,

Fig. 5. Construction stages of the specimens. (a) Foundation construction, (b) Specimen construction, (c) Casting of upper tie beam.

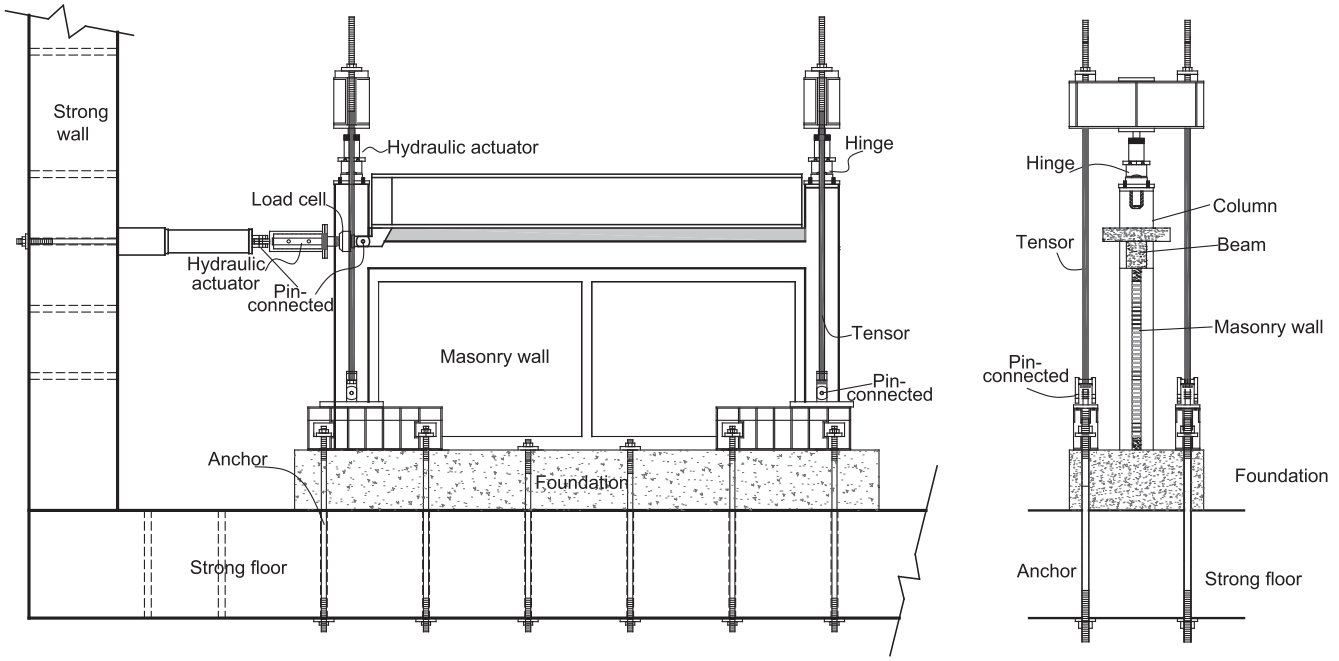

Fig. 6. Experimental setup. (a) Elevation view, (b) Transverse view.

as shown in Fig. 6a. The hydraulic actuators were pin-connected to a steel beam that was bolted to the frame beam so that the lateral load was uniformly transferred to the frame, simulating a seismic load.

Strain gauges and displacement transducers were installed in each specimen to monitor the strains in the reinforcing bars and the deformations of the specimen at different locations, as shown in Fig. 7.

2.6. Load sequence

Testing was initiated with the application of the vertical load on the columns, which was kept constant for the duration of each test. The value of the load was determined based on the analysis of the corresponding prototype building. The application of the vertical load directly to the columns is justified based on two assumptions: (1) the frame and floor are built before the walls so that weight of the upper stories is transferred to the columns and (2) the columns are axially stiffer than the walls. Similar conclusions were drawn in other studies that used similar load setups [3,12]. An elastic analysis using finite-element models of the two prototype buildings showed that the columns in the lower story support more than 98% of the live load.

Vertical loads of 120.17 kN and 245.20 kN were applied on each column of the specimens corresponding to the three- and six-story buildings, respectively. The weight of the steel beam on top of the fame beam was 12.75 kN.

Lateral load was applied according to the test procedure described in appendix A of NTCM-2004. The first two cycles were load controlled up to 25% of the estimated cracking load, the next two cycles up to 50% of the estimated cracking load, and two more up to 100% of the cracking load. The estimated cracking lateral load was 58.86 kN. Subsequently, the tests were displacement controlled. Drifts with increments of 0.002 were applied doing two cycles for each increment.

When the specimen reached a deformation of 0.02 (lateral displacement/wall height) the drift increment changed to 0.004. This change is not specified in the NTCM code, as it was designed mainly for confined masonry walls, not for infill walls.

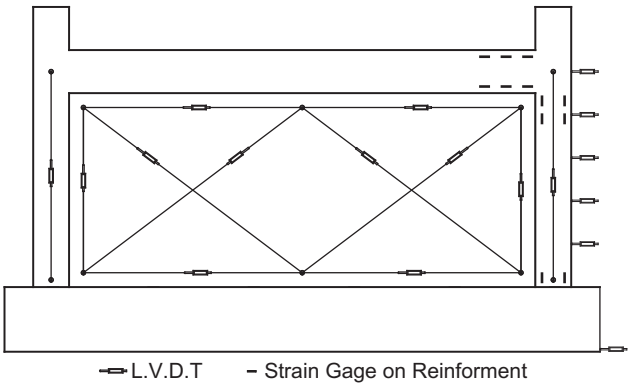

Fig. 7. Instrumentation.

3. Test results

3.1. Wall to frame stiffness ratio

The measure used to characterize the relative stiffness of the frame and the masonry walls is the one proposed by Stafford-Smith and Carter [20]

$$\lambda h = h\sqrt[4]{\frac{E_m t \sin 2\theta}{4E_c I_c h'}} \tag{1}$$

where h is the frame height, E_c is the modulus of elasticity of the concrete used in for the frame columns, I_c is the moment of inertia of the column's section referred to the centroidal axis perpendicular to the plane of the frame, E_m is masonry's the modulus of elasticity and t and h' are the thickness and height of the wall. In this paper, because the change of this ratio is due, mainly, to the column size, we will discussed the observed results in terms of column size instead of the more complex λh parameter. However, it is advised

to use λh in any more formal description of the behavior of any variable with wall to frame stiffness ratio.

3.2. Hysteretic curves

The hysteretic curves are presented in Fig. 8. The stability of the cycles, judged by how well the repeating cycle approximated the first cycle in each displacement increment, in general, is very good. However, it can be observed that the cycles are more stable in the specimens with larger columns. A slow strength degradation was observed in all cases. Pinching of the unloading branch is also present, although it is more pronounced for the specimens with smaller-sized columns. The loading paths intersect the vertical axis, approximately, at the same level of lateral load.

The first specimen tested was MD6N. For that wall, once the drift reached 0.02, a new cycle was tried, searching for failure. However, the LVDT used to measure the lateral drift exhausted its maximum running distance, reaching a drift of 0.0335. Afterwards, the specimen was unloaded (lateral load only) and the device was substituted with a new one with longer capacity. The test was restarted with the negative branch up to 0.0335 to preserve the symmetry of the test. Then, it was decided that the test should continue normally with drift increments of 0.004.

In the case of specimen MD6NRH, there was an oil leak in one of the lateral load actuators. That explains the cycle anomalies near a drift of 0.025. The problem was fixed, and the test continued normally.

3.2.1. Details of specimen MD3NSR

Specimen MD3NSR presented a contraction crack in the wall-to-column interface on both sides of the wall. This crack had a considerable effect on displacements recorded in the shear-displacement curve, as shown in Fig. 9, where the third cycles of the curves for specimens MD3NSR and MD3N are shown. The loop of specimen MD3NSR starts off with a very small slope, meaning that the frame takes almost all the load because the frame is not in direct contact with the wall. When the frame reaches the wall, an abrupt change of stiffness is clearly observed. The gap between wall and frame did not affect the strength, as can be observed by comparison with the loop from specimen MD3N.

3.3. Crack patterns

3.3.1. General observations

The six tested specimens developed similar crack patterns and crack sequences. At an early stage of the tests, separation between wall and frame occurred through cracks in the interface of these elements. As the tests progressed, separation between wall and frame increased. The maximum separation between column and

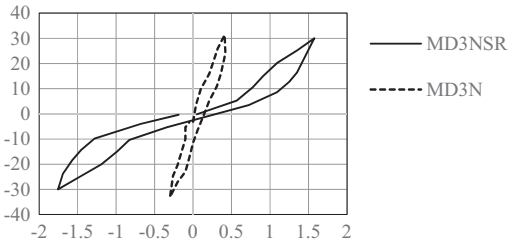

Fig. 9. Force (kN) – Displacement (mm) loops corresponding to the third cycles of specimens MD3NSR and MD3N.

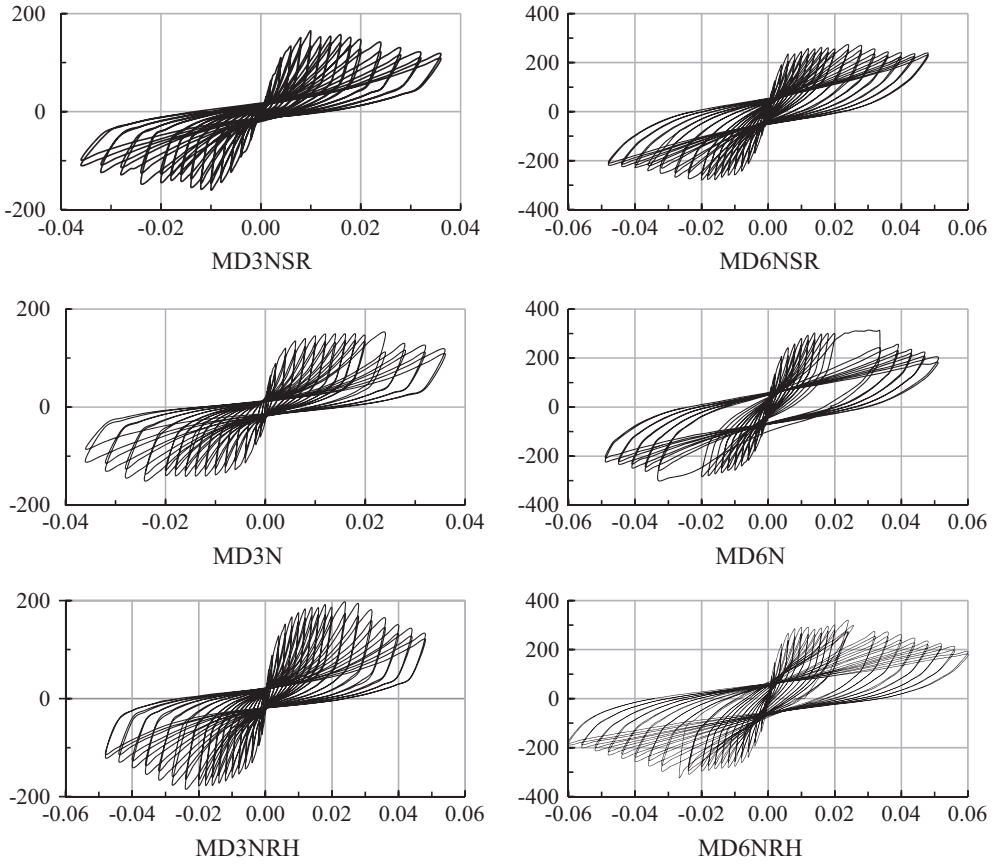

Fig. 8. Lateral Load (kN) – Drift (mm/mm) hysteretic curves.

wall, developed in specimen MD3NSR, was equal to 18 mm. Due to the lateral load, a diagonal strut developed, while separation of the wall and frame occurred at the opposite corners. Gaps between foundation and wall and between wall and frame beam were very thin; however, there was sliding all along the beam-to-wall interface starting very early in the tests.

Separation of the confining elements and the wall was not observed.

3.3.2. Infill-wall cracking

The first diagonal cracking in each specimen was detected by visual inspection. It developed on the central zone of the panel, for specimens with no confining elements, and on the central zone of one of the panels in cases with confining elements. The specimens without confining elements developed a well-defined first inclined crack, while specimens with tie beams and tie columns developed cracking on the wall that was more distributed. The pair of specimens with horizontal reinforcement also had more distributed cracking, when compared to specimens with no horizontal reinforcement.

The drift at the first diagonal cracking for most specimens was 0.0014, which is in good agreement with the drifts at first cracking reported for confined masonry walls in previous studies [13,17]. The values of the lateral load and drift at first diagonal cracking of the specimens are shown in Table 2.

After the first inclined cracking, a combination of inclined cracks and horizontal sliding developed on the wall. As the tests progressed, horizontal sliding was predominant, meaning that few additional inclined cracks developed. In the case of the specimens with confining elements, sliding planes developed every six courses which, for walls with reinforcement, did not coincide with the courses where the horizontal reinforcement was placed. In specimens MD6NSR and MD3NSR, only two main sliding planes formed at the middle height of the wall.

3.3.3. Beam cracking

Cracking at the ends of the beam of the frame occurred at about the same time as the first inclined cracking. The average drift at cracking of the beam was 0.0012, in both specimens with smaller- and larger-sized columns. The corresponding average lateral loads were 61.7 kN and 95.3 kN, respectively. As the test progressed, cracking in the beam extended towards the center of the beam. Fig. 10 shows the cracking and the hysteretic curve of specimen MD3NSR with a drift of 0.0040. Symmetry in the cracking on the wall and the hysteretic curve is observed.

3.3.4. Column cracking

Flexural cracks first appeared at the bottoms of the columns. These cracks developed when the wall was in contact with that zone of the frame, that is, bending was greater at the contact corners. Flexural cracking on the columns extended towards the center of the members as the tests progressed.

In all the specimens with smaller-sized columns, yielding in the longitudinal reinforcement occurred at a drift equal to 0.012, and for specimens with larger-sized columns at a drift equal to 0.010.

In all specimens, a combination of sliding of the infill wall and diagonal tension in the beam-column connection of the frame was the dominant failure mode of the system. The final crack pattern of specimen MD3NRH is shown in Fig. 11, including cracking on the wall and detail of the beam-column connection failure.

3.4. Envelope curves

The envelope curve of specimen MD6N, which is typical, is shown in Fig. 12, along with its critical points: first cracking, (γ_{cr}, V_{cr}), yielding, (γ_{ys}, V_{ys}), maximum strength, (γ_{max}, V_{max}), and failure points, (γ_U, V_U). Usually, cracking is associated with a change in the slope of the envelope curve; however, in these tests, cracking has no apparent effect on the envelope. Changes in the

Table 2
Initial stiffness and shear strength for the critical points of the envelope and elastoplastic model.

Wall	K_i (kN/mm)	K_{in} (kN/mm)	V_y^+ (kN)	V_{cr}^+ (kN)	V_{ys}^+ (kN)	V_{max}^+ (kN)	V_U^+ (kN)	V_{ys}^+/V_{cr}^+	V_{max}^+/V_{yS}^+
MD3NSR	19.68	66.93	145.19	77.99	108.89	162.55	130.04	1.40	1.49
MD3N	88.68	93.26	137.14	76.91	119.38	148.23	118.58	1.55	1.24
MD3NRH	103.73	91.27	178.44	68.57	150.88	194.04	155.23	2.20	1.29
MD6NSR	117.75	100.55	251.23	98.88	233.38	267.71	214.17	2.36	1.15
MD6N	123.88	132.97	288.71	115.36	240.44	311.37	249.10	2.08	1.30
MD6NRH	115.36	130.66	281.15	114.38	264.67	313.72	250.98	2.31	1.19

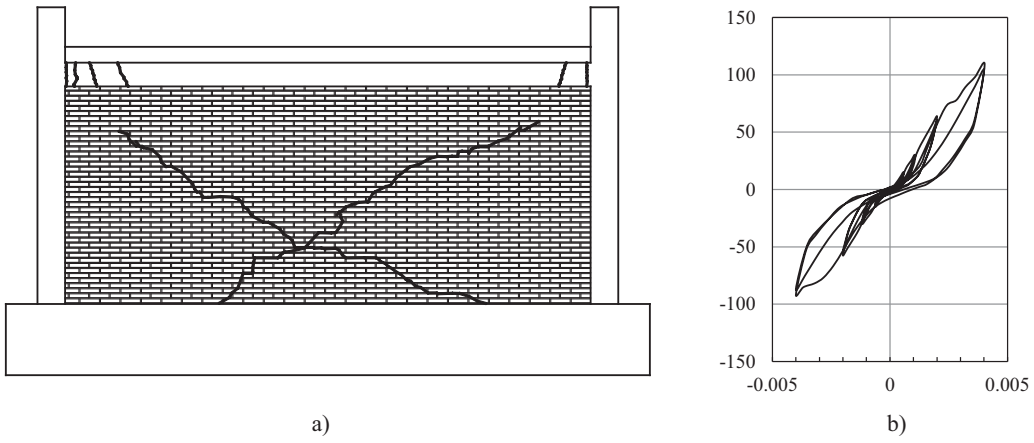

Fig. 10. Results of the test on specimen MD3NSR until drift of 0.004. (a) Crack pattern, (b) Lateral Load (kN) – Drift (mm/mm) hysteretic curve.

a) b)

Fig. 11. Crack pattern of specimen MD3NRH. (a) Cracking on the wall, (b) beam-column connection failure.

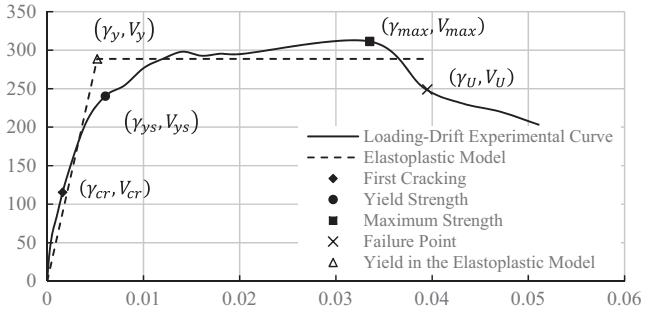

Fig. 12. Lateral Load (kN) – Drift (mm/mm) positive envelope curve of specimen MD6N.

slope (here, the yielding point) of the envelope occur later. Failure of the specimens was defined as a strength decrease to 80% of the maximum strength. The yield point of the equivalent elastoplastic model, (γ_y, V_y), is also shown. The model has the same area under the curve as the experimental envelope and its first branch intersects the experimental envelope at 0.6 V_y. The definition is consistent with FEMA 356 [5], however, an elastoplastic model instead of a bilinear model is sought.

In Table 2, the values of the initial stiffness (K_i) and the lateral loads of the critical points are summarized, while in Table 3, the drifts are given with the ductilities corresponding to the maximum and ultimate strengths.

3.4.1. Initial stiffness

At low levels of lateral displacement, the masonry and frame acted as a monolithic composite structural system. Each loading-drift curve at this stage can be idealized as a straight line whose slope is the initial lateral stiffness, K_i, of the specimen. The initial stiffness was calculated as the slope of the line connecting the maximum point of the first cycle and the origin (Table 2). To have a first estimation of the lateral stiffness of the system, an elastic analysis with finite elements was developed for each model, using the average material mechanical properties presented in Table 1 and a Poisson ratio $\nu = 0.25$ recommended by the Mexican code for analysis [7]. Plane stress panel elements 10 cm wide and 10 cm tall were used to model the walls and confining elements. The stiffnesses of the models (K_{in}) are shown in Table 2.

3.4.2. Cracking strength

The average cracking strength of the specimens with smaller columns was 74.49 kN with a range of [68.57, 77.99], and, for models with larger-sized columns, 109.54 kN with a range of [98.88, 115.36]. The effect of using confining elements was inconsistent for smaller- and larger-column models. In the former group, including confining elements slightly decreased the cracking strength from 77.99 kN with no confining elements to 76.91 kN with confining elements, while in the latter it increased the strength from 98.88 kN to 115.36 kN (a 16.6% increase). However, the effect of reinforcement consistently reduced the cracking strength, from 76.91 to 68.57 for specimens with smaller-size columns and from 115.36 to 114.38 for specimens with lager-size columns. The size of the columns had a considerable effect on the cracking strength: the quotient $V_{cr}(6N)/V_{cr}(3N)$ for the corresponding models with larger and smaller columns was, on average, 1.48. However, the average value of the quotient increased with the use of confining elements, from 1.27 without confining elements to 1.5 with the use of confining elements and to 1.67 with the use of reinforcement.

3.4.3. Yielding

Yielding of the load-drift curve did not occur when the first diagonal cracking was detected. It was not until the first diagonal cracks extended and reached the end of the wall that the yielding in the envelope curve could be observed (Fig. 12).

The yielding strength was, on average, 98.5% larger (V_{ys}/V_{cr} range [1.4, 2.36]) than the cracking strength. The use of confining

Table 3
Drift and ductility of the specimens (mm/mm).

Specimen	γ_y	γ^+_{cr}	γ^+_{ys}	γ^+_{max}	γ^+_U	$\mu_{max}\ \gamma^+_{max}/\gamma_y$	$\mu_U\ \gamma^+_U/\gamma_y$
MD3NSR	0.0051	0.0028	0.0040	0.0100	0.0270	2.0	5.3
MD3N	0.0030	0.0014	0.0040	0.0241	0.0343	8.0	11.4
MD3NRH	0.0050	0.0014	0.0060	0.0241	0.0377	4.8	7.5
MD6NSR	0.0059	0.0014	0.0060	0.0242	0.0442	3.4	7.5
MD6N	0.0052	0.0016	0.0060	0.0335	0.0395	6.4	7.6
MD6NRH	0.0044	0.0014	0.0060	0.0240	0.0412	5.5	9.4

elements did not significantly affect this quotient, which had an average value of 1.82 for infill walls with confining elements and 1.88 for walls with no confining elements. Horizontal reinforcement, however, had a stronger impact on the average value of V_{ys}/V_{cr} : for walls with reinforcement, the average value was 2.26, which is 22.1% larger than the average quotient for walls with no horizontal reinforcement (1.85). The wall/frame stiffness ratio also had a considerable effect on the yielding strength of the system: the average value of the quotient $V_{ys}(6N)/V_{ys}(3N)$ for the corresponding models with larger and smaller columns was 1.97. It also had an impact on the quotient V_{ys}/V_{cr}: in specimens with smaller-sized columns, the average value of that quotient was 1.72, while for specimens with larger-sized columns, it was 2.25, a 31.3% increase.

3.4.4. Shear strength

The maximum shear strength was, on average, 27.5% larger than the yielding strength, (V_{max}/V_{ys} range [1.15, 1.49]), with only a small difference in wall/frame stiffness: the average for specimens with smaller-sized columns was 1.34, and for larger-sized columns, 1.21.

The effect of the confining elements was also unimportant: the average value of V_{max}/V_{ys} for specimens with confining elements was 1.27; while, for those with no confining elements, it was 1.32. The strength of the models with confining elements when compared with the models without them was inconsistent for models with smaller and larger-sized columns. In the former case, decreased 8.8% while in the later increased 16.3% (Table 2).

Specimens with horizontal reinforcement had an average V_{max}/V_{ys} quotient equal to 1.24. However, the strength of the model with smaller sized columns, confining elements and with horizontal reinforcement (3NRH) was 30.9% larger than the strength for the same model without horizontal reinforcement (MD3N). The same comparison for models with larger sized columns gave no change in strength.

The size of the frame elements had a considerable effect on the lateral strength of the system. The average value of the quotient $V_{max}(6N)/V_{max}(3N)$, for the corresponding models with larger and smaller-sized columns, was 1.79, and it was equal to 2.1 for the case of walls with confining elements but no reinforcement.

3.4.5. Strength degradation and ultimate strength

Strength degradation was very slow in all cases, as observed in tests by other authors [3,12]. The process of strength degradation was characterized by the deterioration of the sliding planes, propagation of cracking at the ends of the beam and at the base of the columns, and crushing of the masonry, especially around the corners of the walls, all of which occurred gradually as the drift increased. Failure was considered to have occurred when the strength of the system was reduced to 80% of the maximum strength.

It was observed, after in-plane failure, that the lateral stability of the walls was compromised, especially in those infill walls with no confining elements; however, because no out-of-plane forces were applied, there is no evidence of this in the hysteretic curves.

3.4.6. Drifts and ductility

The ductilities at the maximum strength (μ_{max}) and at the ultimate strength (μ_U) were obtained. The ductility was calculated as the ratio of the drift developed by each specimen to the drift at the yield point of de elastoplastic model. In Table 3, the drifts at the critical points of the envelope curves and the ductilities for each specimen are shown.

Drift at cracking was consistently close to 0.0014, except for the model MD3NSR because of the early separation of the wall and frame mentioned in a previous section. For that reason, MD3NSR's drifts and corresponding ductilities cannot be readily compared with the drifts and ductilities of the other models. Consequently, they were excluded from the comparisons and average values described below.

Drifts at yielding and maximum strength were also very consistent; the former was approximately 0.006 (average 0.0056), and the latter was approximately 0.024 (average 0.0260).

Overall drifts at failure averaged 0.0394 with small differences with column size. In specimens with smaller-sized columns, it was not possible to calculate the effect of the use of confining elements on the displacement capacity due to the above-mentioned gap in specimen MD3NSR; however, for specimens with larger-sized columns the lateral displacement at failure decrease 10.6%. The effect of reinforcement was larger in specimens with smaller-sized columns, with a 9.9% increase, while for larger-sized columns the drift increase was only 4.3%.

In the specimens with confining members, the shear strength of the central tie column had an important role. Those specimens reached their ultimate lateral strength when the central tie column failed after a crack crossed it.

For models with larger-sized columns, the quotient of the ductility of specimens with and without confining elements was at maximum strength $\mu_{max}(6N)/\mu_{max}(6NSR) = 1.57$ and 1.01 at failure. In Fig. 13, the effect of the use of confining elements can be observed.

The ductility demand to achieve the maximum strength had an average value of 5.8 and a range of [4.1, 8.0]. The use of horizontal reinforcement reduced the ductility demand for walls with smaller- and larger-sized columns, from 8.0 (3N) to 4.8 (3NRH) and from 6.4 (6N) to 5.5 (6NRH). The effect of column size was to decrease the ductility demand: $\mu_{max}(6N)/\mu_{max}(3N) = 0.8$, when no horizontal reinforcement was used, while it slightly increased for specimens with horizontal reinforcement, $\mu_{max}(6NRH)/\mu_{max}(3NRH) = 1.13$.

Ductility at failure had an average value of 8.7, with a range of [7.5, 11.4]. The effect of reinforcement was inconsistent, for smaller sized columns it reduce from 11.4 to 7.5 and for larger-sized columns increased from 7.6 to 9.4. Average ductility at failure reduced its value with column size from 9.5 for smaller-sized columns to 8.2 for larger-sized columns.

3.5. Energy dissipation

The energy dissipated by a load cycle was computed as the enclosed-area in the force-deformation diagram. The accumulated dissipated-energy was calculated by cycle as the sum of the dissipated-energy of previous cycles including the one considered and it was associated to the given cycle peak deformation. As there are two cycles with the same peak deformation, two values of dissipated-energy for a given peak deformation were found.

The plots of the accumulated dissipated-energy versus drift grouped by column size are presented in Fig. 14. To have smooth curves, the plotted points correspond to the accumulated dissipated-energy up to the first cycle for a given deformation and, between the points, a linear variation was assumed.

All curves have a slope reduction at a drift of 0.02 due to the change in the test sequence of the drift increment from 0.002 to 0.004. A second change in slope, now increasing, can be observed in specimens MD6N and MD6NRH, due to the changes in the load sequence explained in the section describing the hysteresis curves.

For specimens with smaller sized columns (Fig. 14a), the use of confining elements have very little impact on the dissipated-energy. However, the use of horizontal reinforcement increased the dissipated-energy for a given deformation. The average of the

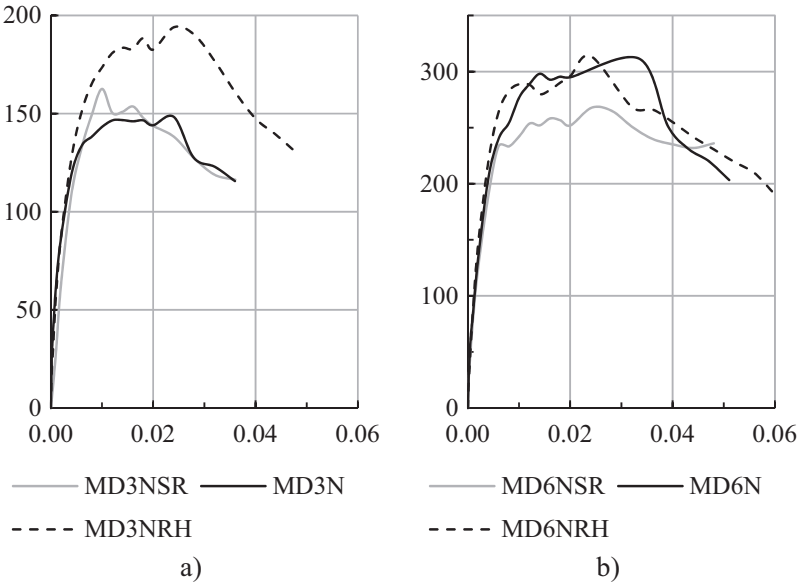

Fig. 13. Lateral Load (kN) – Drift (mm/mm) envelope curves. (a) Specimens with smaller-sized columns, (b) Specimens with larger-sized columns.

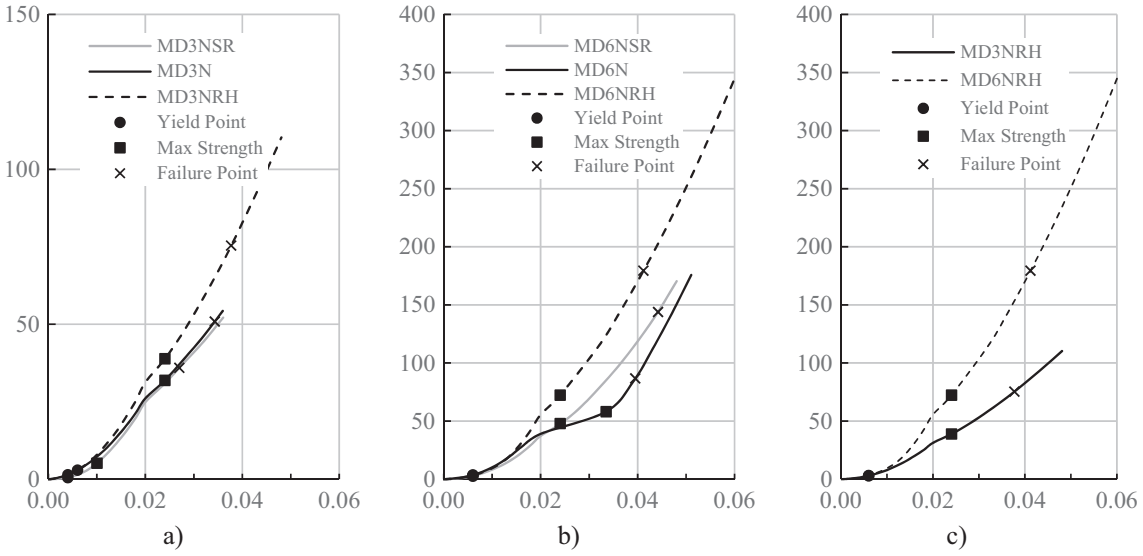

Fig. 14. Accumulated dissipated-energy (J × 103) – Drift (mm/mm). (a) Specimens with smaller size columns, (b) Specimens with larger size columns, (c) Specimens with different size of columns.

3NRH over 3N accumulated dissipated-energy quotient for deformations 0.001 onwards was 1.136 and the range was [0.97, 1.316].

Similarly for specimens with larger-sized columns (Fig. 14b), the effect of confinement before a deformation of 0.02 is negligible The abrupt reduction of dissipated-energy in specimen 6N is due to the equally abrupt change of its lateral deformation from 0.002 to 0.0335, after which, the 6N dissipated-energy tend towards the one of 6NSR. The use of horizontal reinforcement increase the energy dissipated by the system.

Column size contributed significantly to the system's dissipation of energy. The specimens with larger columns dissipated, on average, 1.55 times more energy at a given deformation with a range [0.67, 2.15] (see Table 4).

The comparison of the dissipated-energy of different specimens at the critical points give a different picture. The energy-dissipated at maximum strength for the specimen with smaller-size columns at confinement was $E_d(3N)/E_d(3NSR) = 6.17$ times the energy dissipated by the specimen with no confinement, and at failure was 1.42 times larger. For specimens with larger-sized columns the corresponding quotients were, 1.21 and 0.6.

The effect of reinforcement is that more dissipated energy is needed to reach de maximum strength, for smaller-sized columns was $E_d(3NRH)/E_d(3N) = 1.22$ times larger than that required by the specimen with no reinforcement and at failure 1.48 times larger. The corresponding number for specimens with larger-sized columns were 1.25 and 2.07.

In average the dissipated energy was 2.3 times larger for specimens with larger-sized columns at maximum strength and 2.5 larger at failure.

4. Predictions of design codes

When separation between wall and frame occurred, the wall acted as a diagonal strut and, due to its high stiffness, the masonry

Table 4
Accumulated dissipated energy (E_d) at the critical points (J × 10^3).

Specimen	γ_{ys}	E_d	γ_{max}	E_d	γ_U	E_d
MD3NSR	0.0028	0.52	0.0100	5.17	0.0270	35.94
MD3N	0.0014	1.44	0.0241	31.94	0.0343	50.88
MD3NRH	0.0014	2.94	0.0241	38.90	0.0377	75.42
MD6NSR	0.0014	2.63	0.0242	47.94	0.0442	143.91
MD6N	0.0016	3.73	0.0335	58.14	0.0395	86.78
MD6NRH	0.0014	3.20	0.0240	72.40	0.0412	179.44

Table 5
Braced-frame stiffness from analytical models and experimental results. Values in kN/mm.

Specimen	Stafford-Smith and Carter [20]	Bazán [1]	MSJC [11]	Canadian Standard (2004)	New Zealand Standard (2004)	Experimental infilled-frame stiffness (K_{bf})
MD3NSR						18.02
MD3N	29.83	16.12	10.68	16.63	17.14	19.60
MD3NRH						16.75
MD6NSR						25.91
MD6N	56.43	40.31	32.24	37.00	37.95	26.54
MD6NRH						29.18

Table 6
Shear strength of the horizontal reinforcement, according to codes and experimental results. Values in kN.

Specimen	Canadian Standard (2004)		Mexico City Code (2004)	Experimental Results
MD3N	156.3	Sliding	210.1	148.23
MD3NRH	156.3	Sliding	362.7	194.04
MD6N	338.9	Sliding	455.2	311.37
MD6NRH	338.9	Sliding	785.8	313.72

infill stiffened the flexible frame. However, compared with the first stage of the tests, the stiffness was reduced considerably.

The stiffness of the equivalent strut model was estimated for each specimen, using analytical models proposed by different authors. Contributions of the confining elements and horizontal reinforcement were not considered.

The analytical results were compared against the experimental infilled-frame stiffness (K_{bf}), which was calculated as the slope of the line connecting the yield-strength point and the origin of the envelope curve of each specimen. The results are presented in Table 5. It is observed that the New Zealand Standard had the best agreement for infilled -frame stiffness for specimens with smaller-sized columns, while the Masonry Standards Joint Committee [11] had the best agreement for specimens with larger-sized columns.

The maximum strength to lateral load for each specimen was estimated according to the Canadian Standard [2] and the Mexico City code [7]. The resistance of the system was equal to the force required to reach the maximum strength of the infill wall. Elastic analysis was carried out using the equivalent-diagonal method proposed by the Canadian Standard. The results are shown in Table 6. Experimental results for specimens with and without horizontal reinforcement are also presented.

It is observed that Canadian Standard predicts properly the maximum strength of specimens without horizontal reinforcement, although the error was greater for specimens with larger-sized columns. The percent error was 5.4% for specimens with smaller-sized columns and no reinforcement; however, the prediction was 19.4% lower for the case of specimen MD3NRH. For specimens with larger-sized columns, the errors were 8.8% for specimen MD6N and 8% for model MD6NRH.

According to the Canadian Standard, the failure of the specimens occurs by sliding on the bed joints. Experimental results showed that diagonal cracks developed on the panel, but they were followed by horizontal sliding. As the test progressed, horizontal sliding gained greater importance.

It is observed that the Mexico City code does not predict properly the shear strength of the system, with or without horizontal reinforcement. It greatly overestimates the strength of the system. The Mexico City code does not differentiate between failure modes.

In addition, horizontal reinforcement had a greater contribution to the maximum load in specimens with smaller-sized columns, so the wall/frame stiffness ratio has an important role.

5. Discussion

5.1. Effects of the wall/frame stiffness ratio

Fig. 15 shows that the frame contributes significantly to the lateral strength of the system. On average, for the models with larger columns, the cracking strength was 1.48 times larger, the yielding strength was 1.97 times larger, and the maximum strength was 1.79 times larger, than for the specimens with smaller sized columns.

Regarding the effect of this variable on ductility, it tends to reduce the ductility demand on the system: ductilities of specimens with larger-sized columns were, in average, 17% smaller at the maximum strength and 14% smaller at failure. These results may be explained by the fact that sliding initiated earlier and was predominant on specimens with larger-sized columns; this is a failure mode that is less ductile than the failure mode in which inclined cracking is predominant. Sliding inhibits the formation of new cracks, damage is concentrated in the sliding planes.

The increase of the dissipated-energy with column size is a consequence of the increase in strength, the area enclosed by the load cycles is larger.

5.2. Confining elements

The use of confining elements did not significantly affect the shear strength of the system (Fig. 13). This result is consistent with

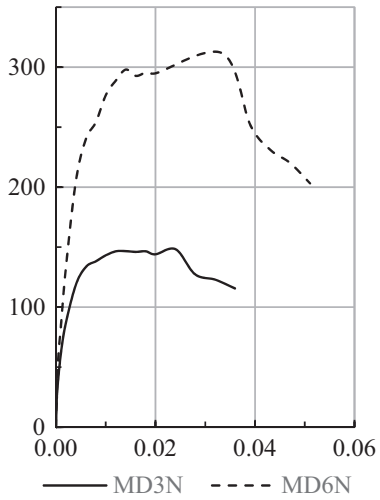

Fig. 15. Lateral Load (kN) – Drift (mm/mm) envelope curves of specimens with different wall/frame stiffness ratios.

the assumption, for the design of confined masonry walls, that no contribution to the shear strength of the wall is attributed to the tie columns. This results is consistent with the fact that there was no significant change on the dissipated-energy at a give deformation.

No significant effect of the use of confining elements was observed in the displacement capacity of the system. However, the ductility demand to reach the maximum strength increase considerably. It seems that the confining elements tend to produce a more efficient strut action in the infill wall that in turn tend to produce more diagonal cracks. This behavior may explain the increase in plastic deformation.

The confining element did contribute to the lateral stability of the walls; however, this is a qualitative observation, as there is no numerical measure to establish the extent of the contribution.

The use of confining elements ensures the contact between wall and frame. Crisafulli [3] recognized that when the frame is built and later infilled by masonry walls, the shrinkage of the infill material or defects due to inaccurate workmanship can result in an initial lack of fit; this was observed with specimen MD3NSR.

5.3. Effects of the horizontal reinforcement

The horizontal reinforcement considerably increased the shear strength of the system after the yield point for specimens with smaller-sized columns. For the case of models with larger-sized columns, no significant change in shear strength was observed. The lack of effect of the horizontal reinforcement in specimens with larger-sized columns is consistent with the fact that larger-sized columns produce a failure mode that predominantly involves sliding, as explained before. Horizontal reinforcement can only be effective if incline cracks cross the reinforcing bars. This is recognized by the Canadian code, which does not include the contribution of the horizontal reinforcement to the shear strength of the infill wall when a sliding failure mode is considered, while the contribution of the horizontal reinforcement is included when diagonal tension is the assumed failure mode.

Reinforcement reduce the ductility demand at maximum strength. This result imply that the specimen had less damage when horizontal reinforcement was provided.

The observed increase of the dissipated energy is, as in the case of column size, the effect of the increase in strength of the system, and is consistent with the fact the increase in dissipated-energy is larger for the specimens with smaller-sized columns, that had a larger increase in strength.

5.4. The special case of MD6N

MD6N's larger drift at maximum strength, compared to the rest of the models, can be explained by the lack of cyclic degradation experienced by that model. As mentioned in the section in which the hysteresis curves were presented, once specimen MD6N reached a drift of 0.02, a new lateral deformation was applied up to 0.0335, which coincided with the maximum strength of the system. Consequently, 22 cycles were skipped (including the repetitions) to reach its strength, compared with the rest of the specimens. A larger number of cycles degrades the strength of the wall [9] and a smaller displacement is necessary to achieve the same strength, and vice versa: fewer cycles imply that a larger displacement is necessary to achieve the same strength. The evidence support the conclusion that the ductility demand to maximum or ultimate strength is sensitive to the load history.

5.5. Predictions of design codes

Diagonal strut models give a good means for the prediction of the lateral stiffness of the system. This is essential to estimate the load on the infill walls. The effects of reinforcement and the use of confining elements on the stiffness of the system are not significant, so ignoring their contributions, as all the strut models do, is reasonable.

The strength of the system provided by the Canadian code is quite good; however, when the horizontal reinforcement contributed significantly, as it did for the case of specimen MD3NRH, a significant variation of the prediction relative to the experimental result was observed. This suggests that the effect of the relative wall/frame stiffness ratio is yet to be understood clearly. The prediction of the strength of the infill wall is not associated with a specific ductility. Thus, while the strength is calculated reasonably well (except in the case mentioned above), nothing about the ductility demand at the maximum strength is indicated.

6. Conclusions

Based on the results of the experimental program, in which six concrete frames are studied with two different column sizes infilled with masonry walls with and without confining elements, and with and without horizontal reinforcement for those with confining elements, the following conclusions can be drawn.

- The shear strength of the infilled framed significantly depends on the strength of the frame.
- Larger frame-to-wall stiffness ratios (here columns size) produce a failure mode that is predominantly a sliding mode. Sliding inhibits the production of new inclined cracks. Damage is concentrated in the sliding planes.
- Confining elements did not have a considerable effect on the shear strength or displacement capacity of the system.
- The confining elements were useful to anchor the horizontal reinforcement and to enhance the out-of-plane stability of the wall, especially at advanced stages of in-plane damage of the infill wall. In addition, confining elements ensure the contact between wall and frame.
- The use of horizontal reinforcement does contribute to the shear strength of the system; however, its efficacy is reduced as the frame-to-wall stiffness ratio increases. The reason for this is related to a previous conclusion: a larger frame-to-wall stiffness ratio results in a wall failure that is predominantly a sliding mode that inhibits the production of new inclined cracks, which are necessary to activate (deform) the horizontal reinforcement.

- Larger frame-to-wall stiffness and the use of horizontal reinforcement reduce the ductility demand of the system at maximum strength.
- An increase of accumulated dissipated energy consistently reflects the increase in strength of the system.
- The available equivalent strut models are adequate to predict the lateral stiffness of the system. This means that the strength demand of the infill walls when subjected to lateral loads can be predicted.
- The lateral strength provided by the Canadian code is adequate in many cases; however, the effect of the wall/frame stiffness ratio on the contribution of the horizontal reinforcement needs to be better understood.
- The available predictions of the lateral strength of the system are not associated with a corresponding ductility. A design method in which the ductility and strength can be related is a requirement for a performance-based design. A design method that meets this requirement is still needed.

Acknowledgements

This investigation was partially funded by CONACYT, which provided the PhD scholarship, and additional funds were provided through the graduate program of UNAM. The funds for the construction of the specimens were provided by PROFAPI of the Autonomous University of Sinaloa (UAS), and the tests were carried out in the Structures Lab of that institution.

References

[1] Bazán ZTE. Muros de Mampostería ante Cargas Laterales PhD Thesis. Mexico D. F.: National Autonomous University of Mexico; 1980.
[2] Canadian Standard Association (CSA). Design of masonry structures, Tech. Rep. CSA S304.1-04, Ontario, Canada; 2004.
[3] Crisafulli FJ. Seismic behavior of reinforced concrete structures with masonry infills PhD Tesis. New Zealand: University of Carterbury; 1997.
[4] Drysdale RG, Hamid AA, Baker LR. Masonry structures: behavior and design. 2nd ed. Boulder, Colorado: The Masonry Society; 1999. 888 pp.
[5] Federal Emergency Management Agency (FEMA). Prestandard and commentary for the seismic rehabilitation of buildings, Tech. Rep. FEMA 356, Washington D.C., USA; 2000.
[6] NTCC. Normas Técnicas Complementarias para diseño y construcción de estructuras de concreto. México: Gobierno del Distrito Federal; 2004.
[7] NTCM. Normas Técnicas Complementarias para diseño y construcción de estructuras de mampostería. México: Gobierno del Distrito Federal; 2004.
[8] Hamburger RO, Meyer JD. The Performance of Steel Frames building with infill masonry walls in the 1906 San Francisco Earthquake. Earthq Spectra 2006;22:43–67.
[9] Ibarra FL, Medina RA, Krawinkler H. Hysteretic models that incorporates strength and stiffness deterioration. Earthquake Eng Struct Dynam 2005;34:1489–511.
[10] Madia FC, Parsekian GA. Modeling a reinforced concrete building frame with infill walls, Paper No. 2.02-2. In: Proceedings, 11th North American Masonry Conference, 5–8 June, 2011, Minneapolis, U.S.A.; 2011.
[11] Masonry Standards Joint Committee (MSJC). MSJC Code/Commentary Working Draft; 2010.
[12] Mehrabi AB, Shing PB, Schuller M, Noland J. Experimental evaluation of masonry-infilled RC frames. ASCE J Struct Eng 1996;122:228–37.
[13] Meli R. Behaviour of Masonry Walls Under Lateral Loads, Paper No. 5_Vol 1_853. In: Proceedings, 5th World Conference on Earthquake Engineering, 25–29 June, 1973, Rome, Italy; 1973.
[14] Murty CVR, Jain SK. Beneficial influence of masonry infill walls on seismic performance of RC frame buildings, Paper No. 1790. In: Proceedings, 12th World Conference on Earthquake Engineering, 2000, Auckland, New Zealand; 2000.
[15] New Zealand Standard (NZS). Design of reinforced concrete masonry structures, Tech. Rep. NZS 4230:2004, Wellington, New Zealand; 2004.
[16] Organismo Nacional de Normalización y Certificación de la Construcción y Edificación (ONNCCE). Determinación de la resistencia a compresión y módulo de elasticidad de pilas de mampostería de arcilla o de concreto, Tech. Rep. NMX-C-464-ONNCCE 2011, México D.F.; 2011.
[17] Pérez-Gavilán JJ, Flores LE, Alcocer SM. An experimental study of confined masonry walls with varying aspect ratios. Earthq Spectra 2015;31:945–68.
[18] Ravichandra SS, Klinger RE. Seismic design factors for steel moment frames with masonry infills: Part 1 and 2, Paper No. 2.02–4 and 2.02-5. In: Proceedings, 11th North American Masonry Conference, 5–8 June, 2011, Minneapolis, U.S.A.; 2011.
[19] Saatcioglu M, Mitchell D, Tinawi R, Garnerd N, Gillies J, Ghobarh A, et al. The August 17, 1999, Kocaeli (Turkey) earthquake- damage to structures. Can J Civ Eng 2001;28:715–37.
[20] Stafford-Smith B, Carter C. A method of analysis for infilled frames. Proc Inst Civ Eng 1969;44:31–48.